



Tensile-strained germanium microdisks with circular Bragg reflectors

M. El Kurdi, M. Prost, A. Ghrib, A. Elbaz, S. Sauvage, X. Checoury, G. Beaudoin, I. Sagnes, G. Picardi, R. Ossikovski, F. Boeuf, and P. Boucaud

Citation: [Applied Physics Letters](#) **108**, 091103 (2016); doi: 10.1063/1.4942891

View online: <http://dx.doi.org/10.1063/1.4942891>

View Table of Contents: <http://scitation.aip.org/content/aip/journal/apl/108/9?ver=pdfcov>

Published by the [AIP Publishing](#)

Articles you may be interested in

[Tensile-strained germanium microdisks](#)

Appl. Phys. Lett. **102**, 221112 (2013); 10.1063/1.4809832

[Rayleigh scattering, mode coupling, and optical loss in silicon microdisks](#)

Appl. Phys. Lett. **85**, 3693 (2004); 10.1063/1.1811378

[Detection of chemical species using ultraviolet microdisk lasers](#)

Appl. Phys. Lett. **85**, 3666 (2004); 10.1063/1.1807967

[Effects of thermal annealing of W/SiO₂ multilayer Bragg reflectors on resonance characteristics of film bulk acoustic resonator devices with cobalt electrodes](#)

J. Vac. Sci. Technol. A **22**, 465 (2004); 10.1116/1.1690248

[High-finesse disk microcavity based on a circular Bragg reflector](#)

Appl. Phys. Lett. **73**, 1314 (1998); 10.1063/1.121880

The advertisement features a blue background with a glowing light effect and a molecular structure. On the left, there is a small image of the journal cover for 'AIP Applied Physics Reviews', which shows a 3D diagram of a layered structure. The main text 'NEW Special Topic Sections' is in large white font. Below it, 'NOW ONLINE' is in yellow, followed by 'Lithium Niobate Properties and Applications: Reviews of Emerging Trends' in white. The AIP Applied Physics Reviews logo is in the bottom right corner.

NEW Special Topic Sections

NOW ONLINE
Lithium Niobate Properties and Applications:
Reviews of Emerging Trends

AIP Applied Physics
Reviews

Tensile-strained germanium microdisks with circular Bragg reflectors

M. El Kurdi,¹ M. Prost,¹ A. Ghrib,¹ A. Elbaz,^{1,a)} S. Sauvage,¹ X. Checoury,¹ G. Beaudoin,² I. Sagnes,² G. Picardi,³ R. Ossikovski,³ F. Boeuf,⁴ and P. Boucaud¹

¹*Institut d'Electronique Fondamentale, CNRS, Univ. Paris-Sud, Université Paris-Saclay, Bâtiment 220, Rue André Ampère, F-91405 Orsay, France*

²*Laboratoire de Photonique et de Nanostructures, CNRS - UPR 20, Route de Nozay, F-91460 Marcoussis, France*

³*Laboratoire de Physique des Interfaces et des Couches Minces, CNRS, Ecole polytechnique, Université Paris-Saclay, F-91128 Palaiseau, France*

⁴*STMicronics, 850 rue Jean Monnet, F-38920 Crolles, France*

(Received 15 January 2016; accepted 16 February 2016; published online 29 February 2016)

We demonstrate the combination of germanium microdisks tensily strained by silicon nitride layers and circular Bragg reflectors. The microdisks with suspended lateral Bragg reflectors form a cavity with quality factors up to 2000 around 2 μm . This represents a key feature to achieve a microlaser with a quasi-direct band gap germanium under a 1.6% biaxial tensile strain. We show that lowering the temperature significantly improves the quality factor of the quasi-radial modes. Linewidth narrowing is observed in a range of weak continuous wave excitation powers. We finally discuss the requirements to achieve lasing with these kind of structures. © 2016 AIP Publishing LLC.

[<http://dx.doi.org/10.1063/1.4942891>]

Achieving a germanium laser is a major issue for silicon photonics as it provides a simple route for monolithic integration of a laser source on silicon chips. To obtain optical gain with bulk Ge at reasonable excitation densities in the kiloAmp or tens of kiloAmps per square centimeter range, it is necessary to apply a significant tensile strain on the Ge active layer. The transfer of tensile strain decreases the energy difference between the zone-center conduction Γ valley and the indirect L valley, while lifting the degeneracy between heavy and light hole bands in the valence band.¹ Both features allow one to obtain a population inversion at a significant reduced current density as compared to bulk Ge.^{2,3} Different methods have been reported in the literature to achieve significant tensile strains, either by mechanically deforming nanomembranes,^{4,5} patterning Ge-on-silicon or on oxide into microbridges,⁶⁻⁸ growing Ge on lattice-mismatched buffer layers,⁹⁻¹¹ or applying external stressor layers like silicon nitride layers.¹²⁻¹⁶ A quasi-direct or direct band gap germanium has been demonstrated by these different methods.^{4,17,18} To achieve lasing, it is also necessary to dispose of a cavity for the optical feedback. Long Fabry-Perot cavities have been used for the ridge lasers.¹⁹ For strongly tensile-strained germanium, the volume where the strain is at maximum is often reduced, and microresonators need to be engineered, for strained microbridges, nanomembranes, or microdisks.²⁰

Germanium microdisks are very attractive structures as they allow to obtain quasi-direct¹⁸ or even direct band gap germanium by applying silicon nitride stressor layers.²¹ This results from the cylindrical symmetry of the microdisks leading to the transfer of large biaxial tensile strains. In a standard microdisk, the Fabry-Perot or quasi-radial modes that propagate along one disk diameter have low quality factors

as the reflectivity provided by a germanium/silicon nitride/air interface is weak (Q factor around 50). A route to improve this quality factor is to embed at the microdisk periphery circular Bragg mirrors that can significantly increase the reflectivity.²² There is a significant challenge to transfer this concept to mushroom-type tensile-strained germanium microdisks as the stress transfer is maximized when germanium is self-standing in air at the periphery. In this letter, we show that it is possible to combine germanium tensily strained by silicon nitride layers and self-standing circular Bragg reflectors at the periphery of the microdisks. A significant increase is observed for the quality factor of the quasi-radial modes, with values up to 2000 at 2 μm wavelength, while keeping the free spectral range almost constant, representing a 40-fold increase as compared to previous results.¹³ This reflectivity increase is controlled by the spectral position of the circular Bragg mirror stop band and by lowering the temperature. We assign precisely the observed modes to quasi-radial modes characterized by their azimuthal and nodal radial planes. At low temperature and low excitation powers, we have observed a linewidth narrowing of the emission that is quenched by the temperature increase in the microdisk as the pump power increases. We finally discuss how lasing could be achieved in such structures.

The studied samples have been fabricated by an all-around approach using the method described in Ref. 18. A 200 nm thick germanium layer is grown on a GaAs substrate. The germanium was n-doped with a doping around 10^{19}cm^{-3} . The Ge layer was first covered by a compressively strained silicon nitride layer (250 nm) and an oxide layer (850 nm) deposited by plasma-enhanced chemical vapor deposition. This structure is then bonded on a silicon host substrate using an Au-Au bonding. After this step, the GaAs wafer is chemically removed. Processing of the microdisk is performed on the bonded sample using standard electron beam lithography tools and plasma etching of the

^{a)}STMicronics, 850 rue Jean Monnet, F-38920 Crolles, France.
Electronic mail: philippe.boucaud@ief.u-psud.fr

germanium. A selective wet underetching of the oxide is performed in order to define the microdisk pedestal. A second silicon nitride stressor layer is then deposited on the top surface and the edges of the microdisks thus leading to an all-around silicon nitride stressor layer. For the fabrication of the circular Bragg reflectors, the process was modified as follows. Trenches were defined at the periphery of the microdisk through a second lithography step before the second nitride deposition. The Ge was partially etched by a shallow etching on a thickness close to 150 nm, thus leaving 50 nm of Ge on top of the bottom silicon nitride layer. The whole structure was then covered by silicon nitride and the surface is partially planarized with 450 or 370 nm thick silicon nitride. The width of the trenches was defined in order to fabricate layers with a thickness close to $\frac{\lambda}{4n_{eff}}$. Figure 1(a) shows a scanning electron microscopy image of the germanium microdisk with the circular Bragg reflectors before the second deposition of the silicon nitride stressor layer. A schematic description of the structure after nitride deposition is shown in Fig. 1(b) while an image of the all-around fully processed sample is shown in Fig. 1(c). The inner disk diameter is 4 μm in Fig. 1(a) and 7 periods of distributed Bragg reflectors can be observed. The pedestal has a diameter close to 3 μm at the interface with the microdisk. The circular Bragg mirrors and part of the microdisk are thus self-suspended, and the mode confinement benefits from the strong index contrast between air and the active layers. The Bragg period was varied between 360 and 390 nm in order to tune the stop band around 2 μm wavelength. For the 360 nm pitch structure, the widths of the trenches are 170 and 190 nm for their parts mostly localized in Ge and silicon nitride, respectively. The corresponding stop band spans the spectral range between 1650 and 2300 nm for TE polarization and 1400–1900 nm for TM-polarization. At 2 μm wavelength, the effective index for the quasi-TE₀ mode in the central stacking is 3.23, while it is 2.37 for the quasi-TM₀ mode.

The strain state of the microdisks was investigated by microRaman measurements in a backscattering configuration.¹³ A peak Raman shift of 6.9 cm^{-1} as compared to the

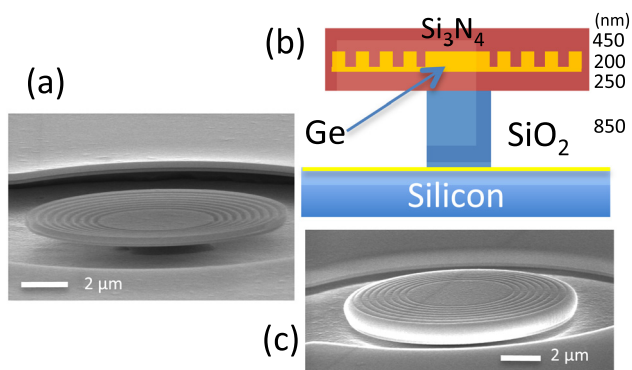


FIG. 1. (a) Scanning electron microscopy image of a tensile-strained germanium microdisk with circular Bragg reflectors. The image is taken before the deposition of the top silicon nitride stressor layer. The SiO_2 pedestal can be observed at the bottom of the microdisk. (b) A schematic diagram of the all-around fully processed sample with the Bragg reflectors. (c) Scanning electron microscopy image of the fully processed sample. The inner disk diameter is 5 μm .

reference Ge on GaAs sample was measured at the center of the microdisk. This Raman shift corresponds to a biaxial strain of 1.59% following the formula $\Delta\omega = -b\varepsilon$, where $b = 415 \text{ cm}^{-1}$ and ε the biaxial strain, if we account for the 0.07% compressive strain of Ge on GaAs used as a reference sample. The strain was partially relaxed in the circular Bragg mirror but it is not detrimental as the active layer is in the central part of the microdisk. With such a strain level, the Ge is still an indirect band gap semiconductor as the crossover between indirect and direct band gap is expected to occur at around 1.7% biaxial strain.²¹ This large strain leads to a significant red-shift of the Ge photoluminescence, and the maximum emission is expected to occur at 2.18 μm at room temperature for the direct recombination involving the Γ conduction band and the light holes and 1.84 μm for the recombination involving the heavy holes.

Figure 2 shows the continuous wave photoluminescence of a 5 μm microdisk with circular Bragg reflectors at room

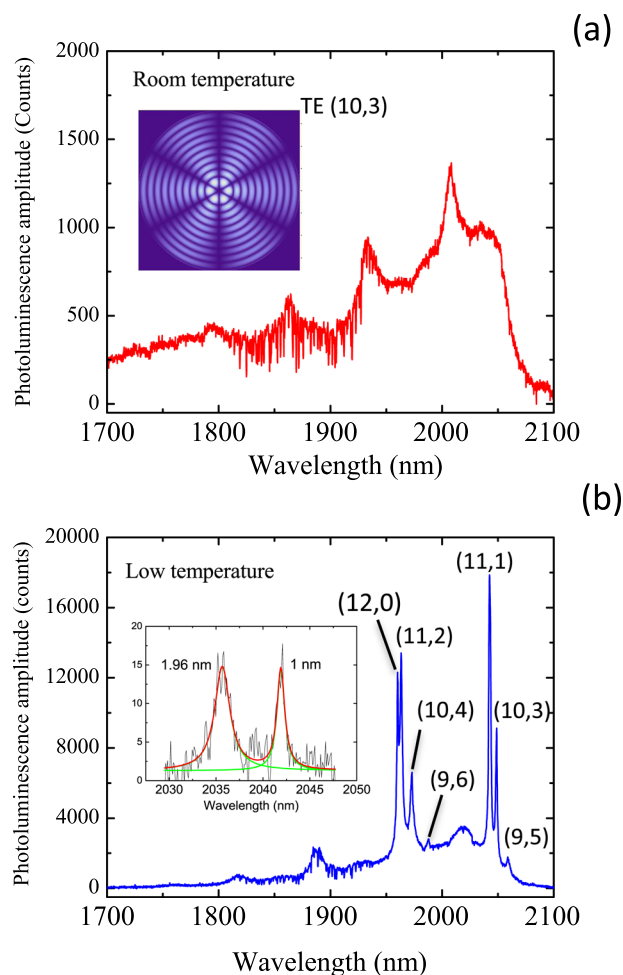


FIG. 2. (a) Top: Room temperature photoluminescence of a 5 μm diameter microdisk with circular Bragg reflectors. The incident power is 3.6 mW ahead of the objective. The inset shows the spatial profile of the TE (10,3) mode evidenced in the Figure (b) below with three azimuthal nodal planes and ten radial nodal circles. (b) Bottom: Low temperature photoluminescence (cryostat setting 8 K). The vertical scale is 10 times higher than in the room temperature measurement. The resonances are labeled according to their radial and azimuthal numbers for the TE₀ family modes. The broad resonance around 2040 nm is attributed to a TM₀ mode. The inset shows a zoom around 2040 nm at weak excitation power (0.25 mW) and the corresponding fits. A 1 nm linewidth corresponds to a Q factor of 2000.

temperature (a) and low temperature (b). The grating pitch is 360 nm. The photoluminescence is excited with a He-Ne laser at 632.8 nm and detected with an extended InGaAs array with a cut-off wavelength at 2070 nm. The spot size has a diameter around 3 μm . A 1 mW power ahead of the objective corresponds to a 10 kW cm⁻² power density incident on the sample. The photoluminescence is collected from the surface perpendicularly to the sample plane using an objective with a numerical aperture of 0.6. In this configuration, the modes that are most easily collected are the quasi-radial modes that strike the disk periphery close to normal incidence as opposed to whispering gallery modes that are localized at the periphery of the microdisk with wave vectors tangential to the disk circumference. The emitted light is guided by the vertical stacking and eventually diffracted at the edges by the Bragg mirrors. We note that these radial modes benefit from the homogeneous strain field in the Ge volume induced by the stressor layers.¹⁸ At room temperature, one observes different family of modes with a free spectral range around 75 nm. These modes stem mostly from the vertically confined TE₀ and TM₀ modes. The linewidth of the resonances remains broad with a lower value of 12 nm around 2000 nm (Q factor of 170). At shorter wavelength, the absorption by the strained Ge layer increases, thus degrading the quality factor of the resonances. The quality factor of the resonances can be significantly improved by decreasing the sample temperature. This is shown in Fig. 2(b) where we also observe the blue shift of the modes as the temperature is decreased. Two main factors explain the improvement of the quality factor: the low temperature leads to a high-energy shift of the strained Ge band gap, thus decreasing the residual absorption that degrades the quality factor around 2 μm . The free carrier and photo-induced near-infrared absorption is also reduced as the temperature is lowered, as a consequence of the reduction of the temperature-dependent lifetime broadening for the intravalley absorption.^{23,24} Coupling of the spontaneous emission to the guided modes might also be modified by the temperature change. At very weak excitation power, a Lorentzian fit of the mode at 2042 nm gives a full width at half maximum of 1 nm, thus corresponding to a quality factor of 2000. It corresponds to 40-fold improvement as compared to a microdisk without circular Bragg reflectors. Note that without Bragg mirrors, the quality factor remains around 50 even at low temperature. At 1961 nm, the lowest measured linewidth was 1.58 nm corresponding to a quality factor of 1200. The family of modes can be identified by using a two-dimensional model where the modes are labeled by their radial and azimuthal numbers n and m .²² In the approximation of quasi-radial modes, the resonance wavelength $\lambda_{n,m}$ is given by the approximate formula^{22,25}

$$\lambda_{n,m} = \frac{2\pi R' n_{\text{eff}}}{\beta_{2n+m}} \left(1 + \frac{4m^2 - 1}{8\beta_{2n+m}^2} \right), \quad (1)$$

where R' is an effective radius (3.55 μm) that accounts for light penetration in the circular Bragg mirror, n the radial number, m the azimuthal number, $\beta_{2n+m} \sim (2n + m - \frac{1}{2}) \frac{\pi}{2}$ when $n \gg m$. β_{2n+m} corresponds to an approximation of the

n th zero of the m th Bessel function when n is much larger than m . The combination of radial and azimuthal numbers explains the splitting of the quasi-radial resonances into three or four-fold modes observed experimentally in Fig. 2(b). We note that the spacing depends on the square of the azimuthal number. The above formula predicts a wavelength spacing of 3 and 12 and 27 nm between the four visible modes around 1960–2000 nm issued from the TE₀ family (12,0), (11,2), (10,4), and (9,6) for the radial and azimuthal numbers. The spacings are experimentally measured at +3 nm, +12.5 nm, and +26 nm, in good agreement with this modeling. A similar agreement is obtained for the modes around 2040 nm.

Figure 3(a) shows the dependence of the photoluminescence spectra as a function of the continuous wave incident pump power. The variation of 1961 nm peak amplitude and

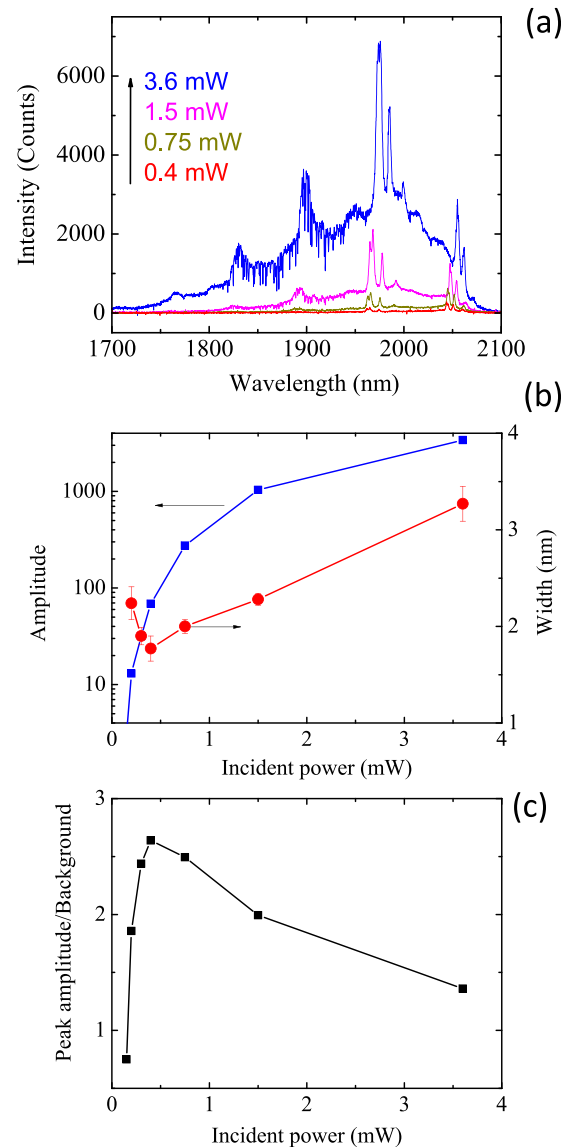


FIG. 3. (a) Top: Low temperature photoluminescence as a function of the incident pump power ahead of the objective. The microdisk has a 5 μm diameter + circular Bragg mirrors (b) Middle: Left scale: Peak amplitude of the resonance at 1961 nm as a function of the pump power. Note the log scale. Right scale: full width at half maximum of the 1961 nm resonance as a function of the pump power. (c) Bottom: Ratio of the resonance peak amplitude to the broad background emission.

its linewidth are shown in Fig. 3(b). The ratio between the peak amplitude and the underlying background is shown in Fig. 3(c). At low excitation, below 0.5 mW, one observes a strong nonlinear increase of the photoluminescence amplitude. The ratio between the resonance amplitude and the background emission also increases significantly. Meanwhile, there is a linewidth reduction of the mode from 2.2 nm down to 1.8 nm. As the pump power is increased above 0.5 mW, the full width at half maximum linewidth starts to increase significantly and the ratio between the resonance amplitude over the background amplitude decreases. A similar behavior measured for quantum dot emission in microdisks has been assigned to lasing.²⁶ Here we do not correlate this behavior with lasing as we would expect that a mode would predominate over the background above threshold as a result of weak value of the spontaneous emission coupling factor for these structures. The linewidth reduction remains however a signature of the decrease of losses and that optical gain occurs in the structures albeit the losses are still dominant. Several features explain that lasing is not achieved. First, there is a significant temperature increase in the microdisk as the pump power is increased.²⁷ We have calculated the temperature in the microdisk using finite element modeling. In these microdisks, the thermal flow is mainly limited by the size of the oxide pedestal (3 μm at the top) and by the thermal conductivity of this oxide layer. Even with a host substrate at 10 K, the microdisk temperature is already as high as 80 K for a 0.5 mW incident pump power. At 3 mW, it can reach 210 K, thus far from the low temperature target. The thermal management in these microdisks is thus a key issue. For a cw optical pumping, one has to find a trade-off on the size of the microdisk pedestal, knowing that a small size enhances the strain transfer from the nitride layers while degrading the thermal cooling of the microdisk. The second limitation of the present configuration is that the stop band of the circular Bragg mirrors is mostly efficient for TE-polarized light. In tensile-strained germanium, at Brillouin zone-center, the net optical gain is dominant for the TM-polarization associated with the light hole band. In TE polarization, the gain is reduced by a factor of 8 due to a lower dipole moment. When the heavy holes are involved, the net optical gain is dominant for TE-polarized light.

We can estimate the mirror reflectivity R from the standard formula $c \frac{\alpha_i + \frac{1}{2} \ln(R^2)}{n} = \frac{2\pi c}{Q\lambda_0}$.²⁸ The measurement shown in the inset of Fig. 2(b) indicates that, at very low excitation, a Q factor of 2000 can be obtained. Assuming that the absorption losses are residual in this low-temperature case, we can estimate a lower bound for the mirror reflectivity of 97.6%. When the pump power is increased to 1 mW, the Q factor of the same mode is decreased down to around 1000, thus indicating that the Q factor of the photo-induced absorption losses is around 2000, i.e., an absorption around 50 cm^{-1} . To achieve lasing with a 5 μm diameter microdisk and a mirror reflectivity of 97.6%, a modal gain of 50 cm^{-1} is required at threshold.²⁹ An incident pump power of 1 mW corresponds to a microdisk temperature around 120 K. In a separate work, we have measured and modeled the temperature dependence of the direct and indirect recombinations in Ge.²¹

We have deduced a 5 ns non-radiative lifetime at this temperature in Ge. This value is in the same range as those reported in Ref. 30. If we account for this non-radiative lifetime value, the photo-induced carrier density in the strained Ge volume is around $2 \times 10^{18} \text{ cm}^{-3}$. It corresponds to a peak material gain of 115 cm^{-1} around 1960 nm in TE polarization at this temperature if we take into account a 25 meV homogeneous broadening for gain calculation.¹⁸ The mode overlap with the strained Ge layer is around 0.7. The calculated modal gain is thus around $0.7 \times (115 - 50) = 45 \text{ cm}^{-1}$. These estimates indicate that we are close from the threshold and justify that we do observe absorption bleaching in Fig. 3(b) through the linewidth narrowing. We note that the non-radiative lifetime might be slightly overestimated³⁰ as they correspond to measurements performed on bulk samples. The properties of this device are however not sufficiently optimized to obtain a clear lasing evidence in continuous wave excitation. If we increase the pump power, the disk temperature increases significantly, thus limiting the increase of the carrier density. Meanwhile, the homogeneous broadening is likely to increase and this feature also lowers the expected gain, thus decreasing the overall efficiency of the process. In a next generation of devices, the mirror reflectivity will be increased for TM-polarized light for which we expect the maximum gain. A better reflectivity should be obtained by strictly matching the trench width with a $\frac{\lambda}{4n_{\text{eff}}}$ width. The microdisk diameter could also be increased while maintaining a strong tensile strain in order to increase the volume of the active region. Finally, undoped germanium should provide a higher modal gain for the 1.6% strain level.³

In conclusion, we have demonstrated that tensile-strained germanium microdisks can be fabricated with self-standing circular Bragg mirrors. These circular Bragg mirrors significantly enhance the reflectivity of quasi-radial modes. We thus obtain a high Q-factor nanophotonic cavity with 1.6% biaxially strained germanium, a strain value close to the one corresponding to the direct band gap crossover. By performing low-temperature photoluminescence measurements, we were able to enhance the quality factors and identify the different families of quasi-radial modes that are experimentally observed. It was shown that the gain is not sufficient to obtain lasing in TE polarization. We have emphasized the importance of thermal management for the microdisks and we have proposed several optimizations that should allow to obtain a microdisk germanium laser for a next generation of devices.

This work was supported by Agence Nationale de la Recherche under GRAAL convention (ANR Blanc call 2011 BS03 00401) and by “Triangle de la Physique” under Gerlas convention. This work is also partially supported by a public grant overseen by the French National Research Agency (ANR) as part of the “Investissements d’Avenir” program (Labex NanoSaclay, reference: ANR-10-LABX-0035). We acknowledge support from the RENATECH network.

¹J. Liu, X. Sun, D. Pan, X. Wang, L. C. Kimerling, T. L. Koch, and J. Michel, *Opt. Express* **15**, 11272 (2007).

²M. El Kurdi, G. Fishman, S. Sauvage, and P. Boucaud, *J. Appl. Phys.* **107**, 013710 (2010).

- ³M. Prost, M. El Kurdi, F. Aniel, N. Zerounian, S. Sauvage, X. Checoury, F. Boeuf, and P. Boucaud, *J. Appl. Phys.* **118**, 125704 (2015).
- ⁴C. Boztug, J. R. Sanchez-Perez, F. F. Sudradjat, R. Jacobson, D. M. Paskiewicz, M. G. Lagally, and R. Paiella, *Small* **9**, 622 (2013).
- ⁵C. Boztug, J. R. Sanchez-Perez, F. Cavallo, M. G. Lagally, and R. Paiella, *ACS Nano* **8**, 3136 (2014).
- ⁶J. M. Suess, R. Geiger, A. Minamisawa, G. Schiefler, J. Frigerio, D. Chrastina, G. Isella, R. Spolenak, J. Faist, and H. Sigg, *Nat. Photonics* **7**, 466 (2013).
- ⁷D. Nam, D. S. Sukhdeo, J.-H. Kang, J. Petykiewicz, J. H. Lee, W. S. Jung, J. Vučković, M. L. Brongersma, and K. C. Saraswat, *Nano Lett.* **13**, 3118 (2013).
- ⁸A. Gassenq, K. Guilloy, G. Osvaldo Dias, N. Pauc, D. Rouchon, J.-M. Hartmann, J. Widiez, S. Tardif, F. Rieutord, J. Escalante, I. Duchemin, Y.-M. Niquet, R. Geiger, T. Zabel, H. Sigg, J. Faist, A. Chelnokov, V. Reboud, and V. Calvo, *Appl. Phys. Lett.* **107**, 191904 (2015).
- ⁹Y. Bai, K. E. Lee, C. Cheng, M. L. Lee, and E. A. Fitzgerald, *J. Appl. Phys.* **104**, 084518 (2008).
- ¹⁰R. Jakomin, M. de Kersauson, M. El Kurdi, L. Largeau, O. Mauguin, G. Beaudoin, S. Sauvage, R. Ossikovski, G. Ndong, M. Chaigneau, I. Sagnes, and P. Boucaud, *Appl. Phys. Lett.* **98**, 091901 (2011).
- ¹¹M. de Kersauson, M. Prost, A. Ghrib, M. El Kurdi, S. Sauvage, G. Beaudoin, L. Largeau, O. Mauguin, R. Jakomin, I. Sagnes, G. Ndong, M. Chaigneau, R. Ossikovski, and P. Boucaud, *J. Appl. Phys.* **113**, 183508 (2013).
- ¹²A. Ghrib, M. de Kersauson, M. El Kurdi, R. Jakomin, G. Beaudoin, S. Sauvage, G. Fishman, G. Ndong, M. Chaigneau, R. Ossikovski, I. Sagnes, and P. Boucaud, *Appl. Phys. Lett.* **100**, 201104 (2012).
- ¹³A. Ghrib, M. El Kurdi, M. de Kersauson, M. Prost, S. Sauvage, X. Checoury, G. Beaudoin, I. Sagnes, and P. Boucaud, *Appl. Phys. Lett.* **102**, 221112 (2013).
- ¹⁴G. Capellini, G. Kozlowski, Y. Yamamoto, M. Lisker, C. Wenger, G. Niu, P. Zaumseil, B. Tillack, A. Ghrib, M. de Kersauson, M. El Kurdi, P. Boucaud, and T. Schroeder, *J. Appl. Phys.* **113**, 013513 (2013).
- ¹⁵P. Boucaud, M. El Kurdi, A. Ghrib, M. Prost, M. de Kersauson, S. Sauvage, F. Aniel, X. Checoury, G. Beaudoin, L. Largeau, I. Sagnes, G. Ndong, M. Chaigneau, and R. Ossikovski, *Photonics Res.* **1**, 102 (2013).
- ¹⁶R. Millar, K. Gallacher, A. Samarelli, J. Frigerio, D. Chrastina, G. Isella, T. Dieing, and D. Paul, *Opt. Express* **23**, 18193 (2015).
- ¹⁷D. S. Sukhdeo, D. Nam, J.-H. Kang, M. L. Brongersma, and K. C. Saraswat, *Photonics Res.* **2**, A8 (2014).
- ¹⁸A. Ghrib, M. El Kurdi, M. Prost, S. Sauvage, X. Checoury, G. Beaudoin, M. Chaigneau, R. Ossikovski, I. Sagnes, and P. Boucaud, *Adv. Opt. Mater.* **3**, 353 (2015).
- ¹⁹J. Liu, X. Sun, R. Camacho-Aguilera, L. C. Kimerling, and J. Michel, *Opt. Lett.* **35**, 679 (2010).
- ²⁰R. Chen, S. Gupta, Y.-C. Huang, Y. Huo, C. W. Rudy, E. Sanchez, Y. Kim, T. I. Kamins, K. C. Saraswat, and J. S. Harris, *Nano Lett.* **14**, 37 (2014).
- ²¹M. El Kurdi, M. Prost, A. Ghrib, S. Sauvage, X. Checoury, G. Beaudoin, I. Sagnes, G. Picardi, R. Ossikovski, and P. Boucaud, "Direct band gap germanium microdisks obtained with silicon nitride stressor layers," *ACS Photonics* (published online, 2016).
- ²²D. Labilloy, H. Benisty, C. Weisbuch, T. F. Krauss, C. J. M. Smith, R. Houdre, and U. Oesterle, *Appl. Phys. Lett.* **73**, 1314 (1998).
- ²³J. B. Arthur, A. C. Baynham, W. Fawcett, and E. G. S. Paige, *Phys. Rev.* **152**, 740 (1966).
- ²⁴M. Nedeljkovic, R. Soref, and G. Mashanovich, *IEEE Photonics J.* **7**, 1 (2015).
- ²⁵A. Elbert, *J. Comput. Appl. Math.* **133**, 65 (2001).
- ²⁶M. Burger, G. Callsen, T. Kure, A. Hoffmann, A. Pawlis, D. Reuter, and D. J. As, *Appl. Phys. Lett.* **103**, 021107 (2013).
- ²⁷P. Boucaud, M. El Kurdi, S. Sauvage, M. de Kersauson, A. Ghrib, and X. Checoury, *Nat. Photonics* **7**, 162 (2013).
- ²⁸M. T. Hill and M. C. Gather, *Nat. Photonics* **8**, 908 (2014).
- ²⁹A. Shaw, B. Roycroft, J. Hegarty, D. Labilloy, H. Benisty, C. Weisbuch, T. F. Krauss, C. J. M. Smith, R. Stanley, R. Houdre, and U. Oesterle, *Appl. Phys. Lett.* **75**, 3051 (1999).
- ³⁰R. Geiger, J. Frigerio, M. J. Suess, D. Chrastina, G. Isella, R. Spolenak, J. Faist, and H. Sigg, *Appl. Phys. Lett.* **104**, 062106 (2014).